Probabilistic Method to Improve the Accuracy of Computer-Integrated Surgical Systems

Tamás Haidegger[1,2]

[1] Antal Bejczy Center for Intelligent Robotics (IROB), EKIK, Óbuda University, Bécsi út 96/b, H-1034 Budapest, Hungary, tamas.haidegger@irob.uni-obuda.hu
[2] Austrian Center for Medical Innovation and Technology (ACMIT), Viktor-Kaplan-str. 2, A-2700 Wiener Neustadt, Austria

Abstract: The technological development of the last decades resulted in the rise of entirely new paradigms in healthcare. Computer-Integrated Surgery (CIS) is providing innovative, minimally invasive solutions to heal complex injuries and diseases. It integrates robotic devices to the treatment delivery phase. By now, well over 6 million successful operations have been accomplished with various systems. In certain critical surgical procedures, where spatial accuracy is a must, physicians extensively rely on the help of CIS, and particularly on intra-operative navigation system. For these, the ways of use, including setup, registration and application accuracy metrics are provided by the manufacturers. Depending on the setup, inherent system errors can accumulate, and lead to significant deviation in position measurements. It is crucial to improve the precision of integrated setups, and to determine the overall task execution error. The stochastic approach proposed here offers an easy and straightforward solution to map and scale the error propagation. Applying pre-operative and on-site simulations, the optimal positioning of the navigation system can be achieved. This results in faster task execution and reduction of the probability of surgical errors. Surgical tracking systems have broader applications in endoscopic surgeries, and the method described in the article can be directly applied to these procedures too. It was tested in silico and on a neurosurgical prototype robot system developed at the Johns Hopkins University. The proposed features together can greatly increase the safety and reliability of all procedures where camera systems are involved, and ease the surgeon's task and potentially reduce operating time.

Keywords: CIS accuracy; Image-Guided Surgery; robotic surgery; error propagation

1 Introduction

1.1 Computer-Integrated Surgery: an Emerging Field

Computer-Integrated Surgery (CIS) is the most commonly used term to cover the entire field of interventional technology, from medical image processing and augmented reality applications to automated tissue ablation [1]. A key domain within is called *Image-Guided Surgery* (IGS), meaning the accurate correlation and mapping of the operative field to a pre-operative image or intra-operative

(e.g., ultrasound, fluoroscopy) data set of the patient, providing freehand navigation, positioning accuracy of equipment or guidance for mechatronic systems [2]. IGS has been primarily used in neurosurgery, pediatrics, orthopedics and also had a major impact in ear, nose and throat (ENT) and maxillofacial reconstruction surgery.

A cornerstone of medical imaging and robotics is registration, that means the spatial alignment of different modalities to determine the position and orientation of the patient in the operating field relative to a virtual data set of the anatomy, e.g., a pre-operative image. The registration should provide a homogeneous transformation matrix that allows the conversion of locations and control signals between different devices [3]. As of today, it is still less common to rely on intra-operative patient data, although successful implementations of magnetic resonance (MR) compatible robotic systems [4] and ultrasound guidance systems exist [5].

While currently the dominating sector is the Robot-Assisted Minimally Invasive Surgery (RAMIS), which means real-time teleoperation of the tools by the surgeon, even in this type of robots, novel features (such as visual overlay, augmented reality fusion, tool tracking) require the exact registration of the patient to the robot and the preoperative data [6]. This is also a key enabling technology towards the (partial) automation of surgery [7].

There are two common ways to perform the registration [8]. For the classical, *frame-based stereotaxis*, a stereotactic frame is mounted to the patient's head prior to the computer tomography (CT) or MR imaging and serves as an fixed coordinate system by which any point of the brain can be referenced.

A recent technique—*frameless stereotaxis*—involves a hand-held surgical probe, and it does not require the rigid head-frame. The probe may be tracked by mechanical, optical, ultrasonic or electromagnetic techniques while touching designated points with it. The transformation between the image space and the tracker coordinates can be computed through fiducial-based or anatomical landmark-based registration, relying on paired-point, surface matching (point-cloud) methods or some kind of hybrid transformation [9]. *Fiducials* are artificial markers, screws or other potential reference points. Natural anatomy features such as point landmarks, ridge curves or surfaces may also be used.

Surgical navigation systems match the two frames and provide the tool coordinates in image space, through the spatial tracking of a *Tool Rigid Body* (TRB). The patient's body must be fixed relative to the mounted reference frame (*Dynamic Reference Base*—DRB), otherwise the registration loses its validity. Intra-operative navigation is commonly achieved with a camera system that is able to track rigid bodies within its workspace. Commercially available systems are typically based on infrared stereotactic cameras and active (flashing LED) or passive (reflective paint-covered) markers.

Within all these domains, data collection at large scale became possible with the introduction of CIS systems, also as an enabler of Machine Learning methods [10]. This opened the case for a completely new field, dubbed Surgical Data

Science [11], which really enables the assessment and benchmarking of CIS systems based on surgical process models [12].

1.2 Motivation

Regardless of the partial success in applications, there are some concerns that prevent CIS technologies from becoming dominant in most of the medical areas. While there is a clear need for accuracy and robust operation for many procedures, the associated high expenses are less tolerated. Several projects turned out to be financial failures, as the high development and production costs can only pay back, when significant market penetration is achieved. In many countries, the state-ran healthcare system cannot support costly robot investments, forming a barrier to their deployment. Furthermore, the development of more complex IGS systems, integrating different components lead to the rise of unforeseen errors. Effective compensation for these spatial inaccuracies are necessary towards the future application of robotic technology in the Operating Room (OR). This has become an explicit requirement toward CIS systems in the new ISO/IEC standards on the basic safety and essential performance of surgical robots [13].

It is crucial to meaningfully describe a system's *application accuracy*. It may be a highly non-linear function of the intrinsic and registration accuracies of the components, therefore requiring special handling. Various error propagation techniques have been proposed in the literature—summarized and further evolved here—to determine system errors as a function of the different integrated components.

2 METHODS

Improvement of the safety and reliability of CIS systems can be achieved through the simulation and testing of their control architecture, generating test sequences for the entire navigation and control architecture, and assessing their accuracy [14].

IGS robot systems are based on the principle that during regular operation, the position of the surgical tool mounted on a robot can be controlled precisely, once its location is known relative to the base (reference) coordinate system . A generic robot-integrated IGS system's schematic diagram is shown in Fig. 1, where the nodes represent control frames and the lines mean homogeneous transformations connecting those. The navigation system (e.g., a camera) is able to track at least two markers; first, the position of the *Dynamic Reference Base*, (i.e., a fiducial anchored to the patient) and second, the *Tool Rigid Body*, attached to the end of the robot. The navigation system is also used to register the pre-operative image of the patient to the DRB with the help of e.g., a hand-held probe and skin-mounted fiducials. Then, the surgical plan can be mapped from pre-operative image space (IMG) to the patient's actual coordinate system in the OR (PAT), then to robot coordinates (ROB). The trackable TRB and the last joint, the *Robot*
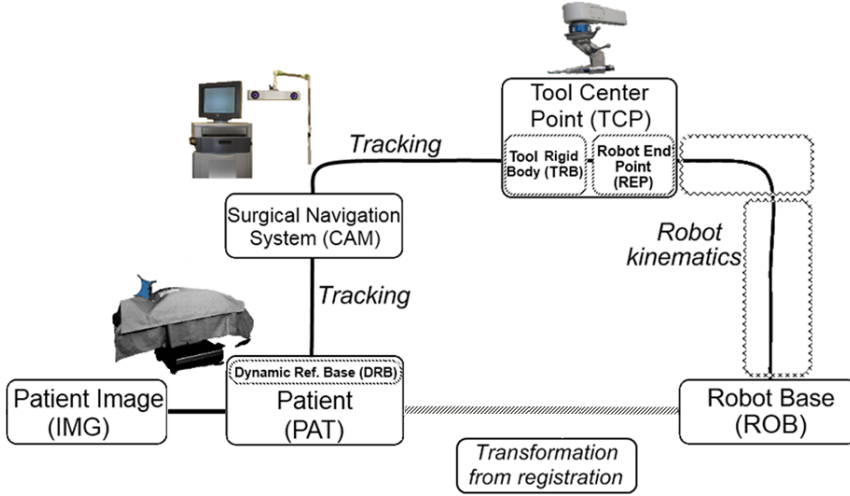
Figure 1
General control concept of IGS robot systems. The solid line represents the typical route of control, while the dashed line is the proposed closed loop approach, relying on the accurate updating of the robot-to-patient registration.

End Point (REP) are different, and the transformation is identified through e.g., pivot calibration. For simplicity, *Tool Center Point* (TCP) is used to denote the end of the robot. The theory of a tracking-based IGS robot was described in [15].

The control signals (Ctrl) generated to move the robot are computed in the IMG frame based on the treatment plan, and then transformed to the Robot base frame (ROB) for execution via the Camera's coordinate frame (CAM):

$$\text{Ctrl}|_{\text{IMG}} = {}^{\text{TCP}}_{\text{ROB}}\mathbf{T} \cdot {}^{\text{CAM}}_{\text{TCP}}\mathbf{T} \cdot {}^{\text{PAT}}_{\text{CAM}}\mathbf{T} \cdot {}^{\text{IMG}}_{\text{PAT}}\mathbf{T} \cdot \text{Ctrl}|_{\text{ROB}}, \tag{1}$$

where $\text{Ctrl}|_{\text{ROB}}$ and $\text{Ctrl}|_{\text{IMG}}$ stand for the control signals expressed in the robot's and the image's frame, respectively. The transformation is in homogeneous coordinates and the Ctrl-s are coordinate values also given as homogeneous vectors. With most IGS systems, the ${}^{\text{PAT}}_{\text{ROB}}\mathbf{T}$ is acquired through registration, and used as a static transformation during the procedure. In Fig. 1, it means closing the control loop (having performed another registration under static conditions):

$$ {}^{\text{PAT}}_{\text{ROB}}\mathbf{T} = {}^{\text{TCP}}_{\text{ROB}}\mathbf{T} \cdot {}^{\text{CAM}}_{\text{TCP}}\mathbf{T} \cdot {}^{\text{PAT}}_{\text{CAM}}\mathbf{T}. \tag{2}$$

2.1 Different Accuracies

It is crucial to properly document the experiments evaluating the usability of a CIS system, especially if it integrates various elements. There are three different types of accuracies (in terms of spatial errors) that can be specified with different error numbers (determined in general) according to [16]:

- intrinsic (technical) accuracy (0.1–0.6 mm),

- registration accuracy (0.2–3 mm),

- application accuracy (0.6–10 mm).

Intrinsic accuracy applies to certain elements, such as the robot or the navigation system. It describes the average error of the given component in operational use. Random errors (e.g., mechanical compliance, friction, loose hardware), resolution of the imaging device, inadequate control and noise can all result in low intrinsic accuracy. On the user interface side, discretized input and modeling errors may further decrease precision.

Registration errors are also present, as computational methods involve some kind of residual errors. In IGS, a major source of error can be the markers (different types, forms and materials), displacement of the fiducials and determination of the center of the fiducials.

Application accuracy refers to the overall targeting error of the integrated system while used in a clinical procedure or a mock setup. It realistically measures the task specific effectiveness of a system and is commonly used for validation. The application accuracy depends on all other sources of errors in a complex, non-linear way, therefore typically phantom, cadaver or clinical trials are required to determine it.

Further problems arise with the simple, ergonomic expression of spatial errors. Physicians may need a single number showing the precision of the system. In many applications, only the absolute distance from a desired location matters, therefore the *root mean square error* (RMSE) is given for the system:

$$E_{\text{RMS}} = \sqrt{\frac{1}{N} \sum_{i=1}^{N} (\mathbf{x}_i - \mathbf{x})^2}, \tag{3}$$

where N is the number of measurements, $\mathbf{x}$ is the desired point and $\mathbf{x}_i$ is the ith measured point. RMSE incorporates both mean and standard deviation values [17]:

$$E_{\text{RMS}}^2 = E_{\text{mean}}^2 + E_{\text{STD}}^2. \tag{4}$$

The RMSE is only an unbiased representation of isotropic and independent errors in the 3D space. For other cases, the covariance matrix of the distribution should be used. Eq. (3) does not incorporate the angular errors of the system, even though any 3D registration or tracking component with a rotational error will affect the translational accuracy. This model is valid for zero-mean Gaussian distributions, and RMSE gives a single value even to multi-dimensional distributions.

Evaluating real robotic systems usually involves not only mathematical modeling and simulation, but also extensive accuracy tests. One of the difficulties in evaluating an IG robot is to acquire the ground truth—the gold standard. This is

feasible through the use of a significantly more precise device (e.g., laser scanner, accurate camera system), the use of a measurement phantom or other trusted method (providing the ground truth).

Most commonly, the medical device is guided (directed) to different positions and orientations along a precisely known set of landmarks (fiducials) or an accuracy board. The positions can also be recorded with an independent localizer.

To evaluate the different point-based tests, certain measures have been developed and used. Let us assume that there are $N + M$ points in total used during the experiment. These can either be artificial fiducials or anatomical landmarks; $\mathbf{p}_1, \mathbf{p}_2, \ldots, \mathbf{p}_N$ points are used during the registration, and $\mathbf{p}_1^*, \mathbf{p}_2^*, \ldots, \mathbf{p}_M^*$ points are used during the procedure (and to derive the error at the target).

Specific to the intra-operative tracker and the setup, the *Fiducial Localization Error* (FLE) includes the intrinsic and extrinsic sources of error, representing the accuracy to localize a $\mathbf{p}_i \, (i = 1, \ldots, N)$ point; consequently the centroid of the cluster of measured points [18] . FLE can be defined as the mean value of the error of all samples:

$$E_{\text{FLE}} = \frac{1}{N_{\text{Fiducial}} M_{\text{Trial}}} \sum_{i=1}^{N_{\text{Fiducial}}} \sum_{j=1}^{M_{\text{Trial}}} \varepsilon(i, j), \tag{5}$$

where ε is the error of a single measurement at a given fiducial. One of the most precise optical trackers available on the market is the *Optotrak Certus* from NDI. It has a 0.1–0.15 mm RMSE FLE according to the specifications. Typical surgical navigation systems provide less accurate measurements, a 0.2–1 mm RMSE error.

Fiducial Registration Error (FRE) is the mean square distance between homologous fiducial points; the residual error of the paired-point registration between the given subset of the known and recorded fiducial coordinates ($\mathbf{p}_i, i = 1, \ldots, N$) during an accuracy test [19]:

$$E_{\text{FRE}} = \sqrt{\frac{1}{N} \sum_{i=1}^{N} \|\mathbf{T}\mathbf{p}_i - \mathbf{q}_i\|^2}, \tag{6}$$

where N is the number of fiducials used during the registration, $\mathbf{q}_i$ is the position of the ith fiducial in one space (may be the robot), $\mathbf{p}_i$ is the same point in the other (patient space) and $\mathbf{T}$ is the computed homogeneous transformation. FRE is connected to FLE [19] through:

$$E_{\text{FRE}}^2 = \left(1 - \frac{1}{2N}\right) E_{\text{FLE}}^2. \tag{7}$$

Target Registration Error (TRE) is the deviation between points ($\mathbf{p}_i^*, i = 1, \ldots, M$) in the reference and the other (registered) coordinate system. FLE, FRE and TRE are presented in Fig. 2. TRE is typically used for the characterization of
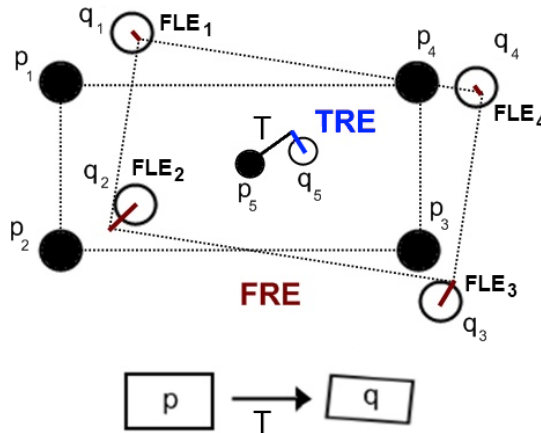
Figure 2
Definition of FRE and TRE to assess point-based registration methods. The black and white circles represent corresponding point pairs in the two different spaces. FLE is the spatial deviation between the true and the recorded position of the landmark points that the registration is built on. FRE is the residual error of the applied transformation calculated over the points used to derive the **T** transformation. TRE is the error of mapping (a set of) independent points from the original space to the registered space [16].

schematic point-based registrations. Ideally, FRE and TRE both equal zero.

$$E_{\text{TRE}} = \sqrt{\frac{1}{M} \sum_{i=1}^{M} \|\mathbf{T}\mathbf{p}_i^* - \mathbf{q}_i\|^2}, \tag{8}$$

where M is the number of fiducials used to compute TRE (that are not identical to any of the points used during registration). In medical cases, TRE might be computed based on distinguished anatomical points. Mean TRE is related to mean FLE through [20]:

$$E_{\text{TRE}}^2(\mathbf{r}) \approx \frac{E_{\text{FLE}}^2}{N} \left(1 + \frac{1}{3} \sum_{i=1}^{3} \frac{d_i^2(\mathbf{r})}{f_i^2} \right), \tag{9}$$

where $\mathbf{r}$ is the target point, N the number of fiducials, $d_i(\cdot)$ the distance of the target from the axis i of the fiducial points and f_i is the RMSE distance of all the fiducial points from that same axis. Novel research publications show that TRE and FRE are independent for point-based registrations, therefore (9) can only be used to estimate TRE for a given fiducial configuration and a defined target position [20, 21] . The FRE in a particular case does not correlate with TRE for any arbitrary chosen configuration. Many commercially available surgical navigation systems use (incorrectly) FRE as a metric for the precision of the system, while others use proprietary algorithms to define an accuracy number to display to the surgeon.

Different research groups defined further types of errors to better describe their models or procedures [22]:

- *Image Plane Error* (IPE) is the measurement error of the camera sensor. It contains the focus, distortions and other imperfections of the lens through the extrinsic and intrinsic camera parameters,

- *Calculated Registration Error* (CRE) is the correlation of pre-operative image and intra-operative anatomical data,

- *Mean Fiducial Error* (MFE) is similar to CRE, using fiducials for registration,

- *Mean Target Error* (MTE) represents the 6 DOF error of a rigid tracking target in the centroid of the fiducials. Its value depends on the FLE of each fiducial and the spatial arrangement of the tracking target,

- *Target Positioning Error* (TPE) is the spatial mismatch between the position of the device and the surgical target that incorporates TRE plus confounders in clinical use.

- *Target Localization Error* (TLE) is the spatial mismatch between the reported position of the device versus its ideal location.

- *Total Targeting Error* (TTE) is the overall error. For the RMSE values, $E_{\text{TTE}}^2 = E_{\text{TRE}}^2 + E_{\text{TLE}}^2$.

More recently, iterative solutions have been developed to solve the *absolute position/orientation problem* in registration, since the need to define better accuracy metrics has gained more attention in the international research community [23, 24].

3 System Error Estimation Concepts

Validation and assessment of image-guided robotic systems can be cumbersome, thus significant effort has been invested into metrology and standards development by the research community. Deterministic spatial accuracy analysis of image registration and surgical robot systems was performed by many research groups [13, 25–28]. Stochastic analysis has mostly been avoided due to the fact that it is computationally demanding and can lead to extremely complex solutions.

A major challenge is to find the best homogeneous transformation that accurately registers matching point pairs in two different data sets. Different metrics, such as the FLE, FRE and TRE have been defined beforehand, and this article describes a new, stochastic approach to deal with the imperfections of an integrated system in a practical manner.

3.1 Accuracy Assessment of Integrated Systems

One of the typical assumptions of the benchmarking methods (based on the *central limit theorem*) is to use Gaussian distribution to model the noise of the original measurements. Focusing solely on registration error estimation, Moghari et al. [29] compares the different noise models found in literature. It is concluded that all the algorithms can be unified through the model presented in [30] that assumes inhomogeneous and anisotropic zero-mean Gaussian noise. For the modeling of navigational devices, identical, isotropic, zero-mean Gaussian noise is used most commonly [31, 32] , although some measurements suggest that the noise may be different for all existing surgical navigation systems [33] . The manufacturers claim to improve on homogeneity continuously, therefore identical distribution will be assumed hereafter. First, let us review previously developed solutions for error estimation, to be able to present their limitations and shortfalls.

3.1.1 Erroneous Transformation Matrix Calculation

The most generic form describing the geometric relation between point clouds for IGS has been derived in the early 1990s. In IG therapy, usually only the positional error is indicated, as the accuracy of the treatment delivery—in these applications—depends on the 3D spatial error [28]. Let us assume that we only have an erroneous ${}^{A}_{B}\widetilde{\mathbf{T}}$ approximation of the ideal ${}^{A}_{B}\mathbf{T}$ transformation:

$$ {}^{A}_{B}\widetilde{\mathbf{T}} = {}^{A}_{B}\mathbf{T} \cdot \Delta^{A}_{B}\mathbf{T} \text{ and } \Delta^{A}_{B}\mathbf{T}_{\text{Rot}} \approx \mathbf{I} + \theta\mathbf{N}, \tag{10} $$

where $\mathbf{I} + \theta\mathbf{N}$ is a first-order Taylor series approximation of a rotation expressed with an angle (θ) around a given axis $\mathbf{n} = [n_x, n_y, n_z]$, $\mathbf{I}$ being the identity matrix:

$$ {}^{A}_{B}\mathbf{T}_{\text{Rot}}(\mathbf{n}, \theta) = e^{\theta\mathbf{N}}, \text{ where } \mathbf{N} = \begin{bmatrix} 0 & -n_z & n_y \\ n_z & 0 & -n_x \\ -n_y & n_x & 0 \end{bmatrix}. \tag{11} $$

A measured $\tilde{x}_A$ value is the approximation of a real x_A,

$$ \tilde{\mathbf{x}}_A = \mathbf{x}_A + \Delta\mathbf{x}_A, \tag{12} $$

then the transformed value derives to be:

$$ \tilde{\mathbf{x}}_B = {}^{A}_{B}\widetilde{\mathbf{T}}\mathbf{x}_A = \mathbf{x}_B + \Delta\mathbf{x}_B, \tag{13} $$

with uncertainty:

$$ \Delta\mathbf{x}_B = {}^{A}_{B}\mathbf{T}_{\text{Rot}}\left(\theta\mathbf{N}\mathbf{x}_A + \Delta\mathbf{x}_A + \Delta^{A}_{B}\mathbf{T}_{\text{Trans}}\right). \tag{14} $$

The disturbance effect of small rotations on small translations is neglected:

$$ \Delta^{A}_{B}\mathbf{T}_{\text{Rot}} \cdot \Delta^{A}_{B}\mathbf{T}_{\text{Trans}} \approx \Delta^{A}_{B}\mathbf{T}_{\text{Trans}}. \tag{15} $$

This method analytically calculates position error accumulation; however, it may be difficult to compute and not accurate enough for certain applications (due to the Taylor series approximation).

3.1.2   Covariance Matrix Based Approximation

It is possible to use a computed estimate of the steady-state error covariance of a system to determine its accuracy [34] . This means that given the vector of the state variables $\mathbf{x}_1, \mathbf{x}_2, \ldots, \mathbf{x}_k$, the error covariance can be determined for every measurement point:

$$\mathbf{\Sigma}_{\mathbf{x}_i} = \mathrm{E}\{\Delta\mathbf{x}_i \Delta\mathbf{x}_i^{\mathrm{T}}\} = \mathrm{E}\{(\mathbf{x}_i - \tilde{\mathbf{x}}_i)(\mathbf{x}_i - \tilde{\mathbf{x}}_i)^{\mathrm{T}}\}, \tag{16}$$

where $\mathbf{x}_i$ and $\tilde{\mathbf{x}}_i$ represents the true and estimated states at point i, respectively. The noise distribution of each point $\mathbf{x}_i$ is given by the covariance matrix $\mathbf{\Sigma}_{\mathbf{x}_i}$. There are different methods to estimate $\mathbf{\Sigma}_{\mathbf{x}_i}$ directly from state-space models through e.g., the closed-formed solution of the discrete algebraic Riccati equation [34] . The limitation of the method is that it requires an accurate model of the system and a larger number of a priori measurements. Let us assume that $\mathbf{x}_B = f(\mathbf{x}_A, \mathbf{t})$, where $\mathbf{t}$ is the representation of the position and orientation. Then a linearized solution can be given to (14):

$$\Delta\mathbf{x}_B = \left.\frac{\partial f(\mathbf{x}_A, \mathbf{t})}{\partial\mathbf{t}}\right|_{\mathbf{t}=\tilde{\mathbf{t}}} = \mathbf{J}_f \Delta\mathbf{t}, \tag{17}$$

where $\mathbf{J}_f$ is the Jacobian matrix (first-order Taylor series approximation) of function f [35] . It is possible to acquire the least squares solution for $\Delta\mathbf{t}$ through:

$$\Delta\mathbf{t} = (\mathbf{J}_f^{\mathrm{T}}\mathbf{J}_f)^{-1}\mathbf{J}_f^{\mathrm{T}}\Delta\mathbf{x}_B. \tag{18}$$

The covariance of $\mathbf{t}$ is given by the expected value of the outer product:

$$\begin{aligned}
\mathbf{\Sigma}_{\mathbf{t}} &= \mathrm{E}\{\Delta\mathbf{t}\Delta\mathbf{t}^{\mathrm{T}}\} \\
&= (\mathbf{J}_f^{\mathrm{T}}\mathbf{J}_f)^{-1}\mathbf{J}_f^{\mathrm{T}}\bar{\mathbf{\Sigma}}_{\mathbf{x}_B}\left((\mathbf{J}_f^{\mathrm{T}}\mathbf{J}_f)^{-1}\mathbf{J}_f^{\mathrm{T}}\right)^{\mathrm{T}},
\end{aligned} \tag{19}$$

where $\bar{\mathbf{\Sigma}}_{\mathbf{x}_B}$ is constructed from the covariance matrices of $\mathbf{x}_B$.

3.1.3   Covariance Propagation

Instead of measuring the covariance of the system separately, it can also be calculated with backward and forward propagation through the approximation of the non-linear, affine coordinate transformations according to [36, 37] . Given (17), the covariance matrix $\mathbf{\Sigma}_f$ can be determined:

$$\mathbf{\Sigma}_f = \mathrm{E}\{(\mathbf{J}_f\Delta\mathbf{x}_A)(\mathbf{J}_f\Delta\mathbf{x}_A)^{\mathrm{T}}\} = \mathbf{J}_f\mathbf{\Sigma}_{\mathbf{x}_A}\mathbf{J}_f^{\mathrm{T}}, \tag{20}$$

If the covariance of $\mathbf{x}_B$ is known, backward propagation can be used, which means employing (20) on the inverse f function:

$$\boldsymbol{\Sigma}_{f^{-1}} = \mathbf{J}_{f^{-1}} \boldsymbol{\Sigma}_{\mathbf{x}_A} \mathbf{J}_{f^{-1}}^{\mathrm{T}} = (\mathbf{J}_f^{\mathrm{T}} \boldsymbol{\Sigma}_{\mathbf{x}_A}^{-1} \mathbf{J}_f)^{-1}. \tag{21}$$

Pseudo-inverse methods can be applied to get the solution for overparametrized cases. With the help of (20) and (21) it is possible to compute the covariance at a Point of Interest (POI) through the known homogeneous transformations leading to the target point from the original base frame.

This form of description allows us to analytically derive the errors in different frames and representations. An example is the computation of the following errors [36]:

- deriving the 2D covariance matrix of a single camera image of a navigation system,

- propagating the error to 3D FLE error based on a camera model,

- deriving the 6D rigid body error based on the FLE,

- propagating the rigid body error to the POI to derive the 3D TRE.

The advantage of this approach is that it allows to build up the whole computation from the lowest level of errors within the imaging system (that may originate in internal camera calibration inaccuracies, imperfect lenses, inaccurate computational algorithms or image blur). However, usually very limited information is available about a navigation system at this level of details, therefore the simplified models applied may end up contributing the similar amount of distortion in the computation than empirically derived higher-level models would.

4 Stochastic Modeling of Complex System Noise

A serious limitation of the above described methods is that most of them do not deal with the orientation error at a target, and does not provide any information about the error distribution. Throughout the article it is assumed that errors or accuracies have Gaussian distribution, which is in some cases not valid. Originally, the concept of coordinate frame registration handled accuracy as a norm of the deviation in x, y, z from the target point—entirely disregarding the orientation uncertainty. In several applications, such as an IG interventional robot applying virtual spatial constraints (such as Virtual Fixtures – VF), it is critical to consider rotational errors as well. The orientation error is considered only from the point of forbidden regions, not including the required accuracy of the approach direction (i.e., the surgical technique).
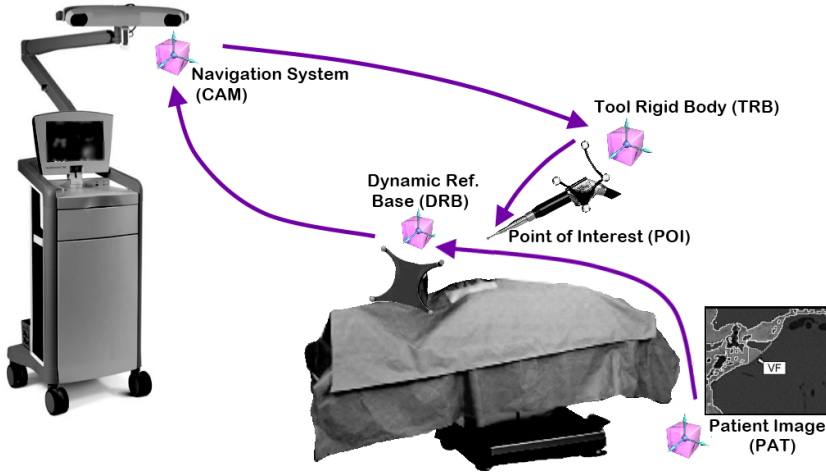
Figure 3
Basic setup of IGS procedures, showing the different coordinate frames used in control to determine
the tool's position
relative to the pre-operative image.

4.1   Theory of Complex Errors

Let us consider a system where the Point of Interest is tracked with an intra-operative navigation system (with any modality). The Dynamic Reference Base is rigidly attached to the patient, and registered to the pre-operative image through any registrational method, with a known angular and translational residual error. The markers (enabling tracking) on the tool are determining a certain coordinate frame—Tool Rigid Body—that is connected to the POI through another transformation acquired from e.g., a pivot calibration, again with known error statistics. The goal is to transform the spatial constraints (e.g., Virtual Fixture) defined in the registered pre-operative image space to the POI in real/time by the set of homogeneous transformations. Let us note that in the case of a typical robotic IGS system the POI corresponds to the Tool Center Point. Fig. 3 shows the general arrangement of the setup. VF defined in the PAT frame can be acquired in the POI frame using the following chain of homogeneous transformations:

$$_{\text{POI}}^{\text{PAT}}\mathbf{T} = {}_{\text{POI}}^{\text{TRB}}\mathbf{T} \cdot {}_{\text{TRB}}^{\text{CAM}}\mathbf{T} \cdot {}_{\text{CAM}}^{\text{DRB}}\mathbf{T} \cdot {}_{\text{DRB}}^{\text{PAT}}\mathbf{T}. \tag{22}$$

It is typically assumed that all terms have known Gaussian distribution, therefore the probability distribution of the POI is anisotropic Gaussian with density function $f(\cdot)$ [14]. The overall transformation can be expressed as the function of the ideal and noise terms:

$$_{\text{POI}}^{\text{PAT}}\mathbf{T} = f(\mathbf{t}) + f(\Delta\mathbf{t}), \tag{23}$$

and it is necessary to express $f(\Delta \mathbf{t})$ for the setup in a simple and effective way. The VF can be described with a convex hull [38] , and the probability $\mathbf{P}(\text{POI} \notin \text{VF})$ that the POI is in the forbidden region can be analytically calculated as:

$$\mathbf{P}(\text{POI} \notin \text{VF}) = \int\limits_{\mathbf{t} \notin \text{VF}} f(\mathbf{t})\, d\mathbf{t}. \qquad (24)$$

It is possible to apply a stochastic approach through (24) to determine the location of the tooltip. This can be considered as the general extension of the approach proposed in [32] . Once we have the VF definitions transformed to the POI's coordinate system, we can derive the exact probability of the tool hitting the forbidden region. Current computational devices allow for the handling of these functions.

Similarly to $\mathbf{P}(\text{POI} \notin \text{VF}_1)$, let us denote by $\mathbf{P}(\text{POI} \notin \text{VF}_2)$ the probability that the POI is deeply in the forbidden sector (beyond a given threshold). An η penalty function—to control the device delivering the treatment—can be built by arbitrary weighting coefficients or functions ($\mathbf{w}$) tailored to the application. We can derive η by integrating the density function within the different VFs and scale it with $\mathbf{w}$. In a practical case, significant errors occurring with lower probability can be considered as:

$$\eta = w_1 \mathbf{P}(\text{POI} \notin \text{VF}_1) + w_2 \mathbf{P}(\text{POI} \notin \text{VF}_2), \qquad (25)$$

where $w_1 > w_2$, if VF_1 is more limiting than VF_2. The whole concept can be extended to incorporate more regions.

In addition, the angular distribution can also provide information about the probability that the POI is moving toward the VF. This is critical e.g., in automated bone drilling tasks. The exact calculation of the probability of the error gives a much stricter control over the motion of the tool, resulting in higher accuracy and safety.

An important feature of the proposed method is implicitly managing a previously challenging case: critical errors with low probability. With the help of differently chosen VF segments and $\mathbf{w}$ factors, any complex constraint function can be built and applied to the IG system in real-time during the execution of the operation.

4.2   Deployment of the Concept

The above presented method has several advantages. It can be applied to IGS systems during the setup phase to verify the performance of the devices in the actual OR arrangement. The manufacturer should provide the generic accuracy numbers of the tracking device and the robot system or these can be acquired pre-operatively. This is especially useful in the case when pre-operatively defined control features are applied, such as Virtual Fixtures.

At the beginning of the surgical procedure, when the devices are roughly positioned around the patient, the simple reading of the actual position information can serve as the input for the simulation. The stochastic method provides the error distribution based on the Monte Carlo simulation in a very short time, and with that knowledge, the surgeon can decide to re-arrange the setup or proceed with the operation.

The algorithm can be extended to call for re-assessment if the devices are significantly relocated compared to the original location. (E.g., the camera is pulled to the opposite side of the room.) However, this seldom happens in the case of real surgeries, where the physicians typically follow a pre-defined protocol.

4.3   Simulation Results

Simulations were performed to verify the concept. An IG bone drilling setup has been simulated (based on Fig. 3) with the parameters of an anthropomorphic robotic arm and a typical OR setup with an optical navigation system. A simplified VF was used to protect a certain region of the patient, while the robot operates in the proximity of it. The actual parameters were chosen to mimic the NeuroMate (commercially available) robot from Renishaw (Wotton-under-Edge, UK), and the registrations were defined based on multiple dry-lab tests. The distribution of the POI's error was acquired with Monte Carlo simulation using 20,000 samples (Fig. 4 (a–h)). Numeric results were derived for test cases, where one VF was a 0.2 mm radius sphere and another was a 0.4 mm radius sphere (Fig. 5), corresponding to a very delicate operation, e.g., the acoustic nerve during a hemifacial spasm treatment via suboccipital approach, pedicle screw placement or laser osteotomy on the sternum. Results showed that the method was effective by providing the probabilities, and showed great flexibility in application. The reason for the extreme-scale anisotropy of the final distribution is the further displacement of the camera base, which is absolutely necessary in a real OR arrangement.

4.4   Error Modeling for Faster Surgical Execution

The main collateral advantage of the new approach is to allow for the a priori estimation of the POI's distribution. Based solely on the devices' known intrinsic accuracy parameters and the registration values (acquired before the surgical procedure) thorough error distribution estimation can be performed. Unless the OR setup changes, this simulation leads to better approximation of the surgical tool's position. With the known anisotropic Gaussian distribution, it is possible to determine which directions are more dangerous from the application point of view (where the STD is larger). The robot can be allowed to move faster towards directions with lower error distribution.

Fig. 6 shows the differences in the distribution of the POI along different axes. The ratio of the STDs along the principal axes can be tenfold, even with the original distributions being isotropic. Principal component analysis showed that two components account for 98% of the variance. This means that if the typical
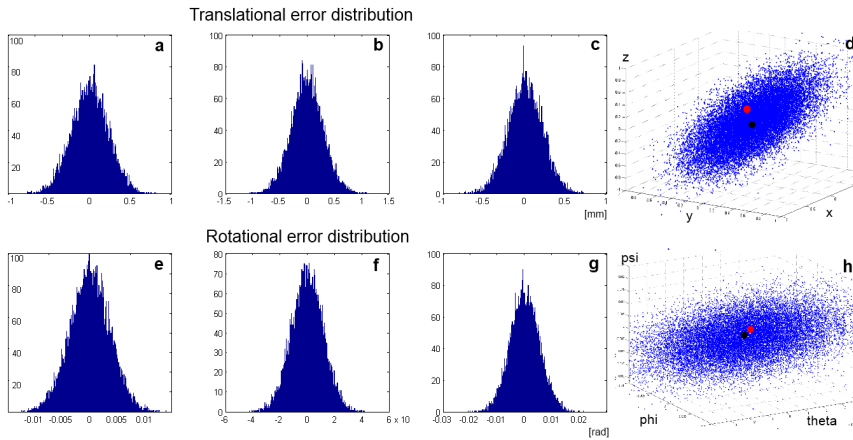
Figure 4

Distribution of the Point of Interest with a simulated IGS system. (a–c) Distribution of position (compared to the deterministic approach); [0.32, 028, 0.30] mm STD along x, y, z, respectively. (d) 3D plot of the translational error. Red dot shows the theoretical position, black dot represents the effect of the registrational errors, i.e., the position estimation according to the classical deterministic method. (e–g) [0.0023, 0.0027, 0.0051] rad STD rotation error around x, y, z, respectively. (h) 3D plot of the angular errors along $[\phi, \theta, \psi]$

.
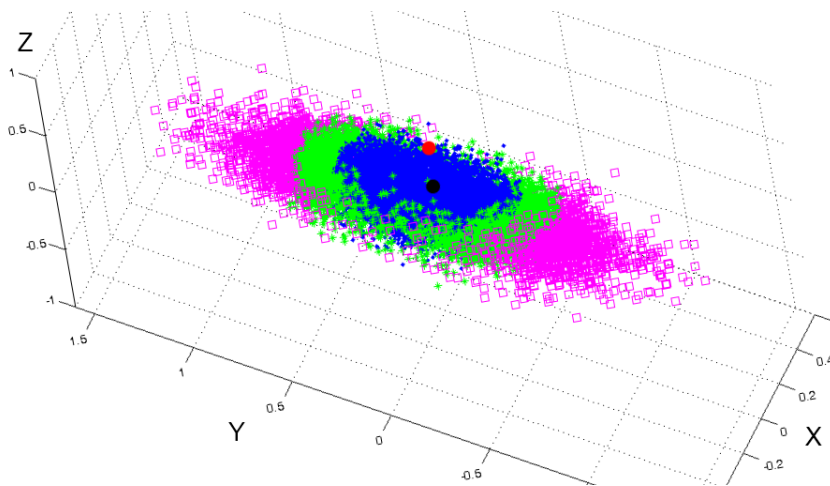
Figure 5

The POI (tooltip) transformed to the coordinate space of the patient. Green stars show where the overall RMSE error is larger than 0.2 mm and magenta squares mark the region where the error is over 0.4 mm. The exact probability of the POI being beyond the VF is 0.438 and 0.214 for the 0.2 and 0.4 mm VF, respectively. The red dot shows the theoretical position, the black dot represents the effect of the registration errors. The point-cloud is shown from an angle from where its anisotropic distribution is most apparent.
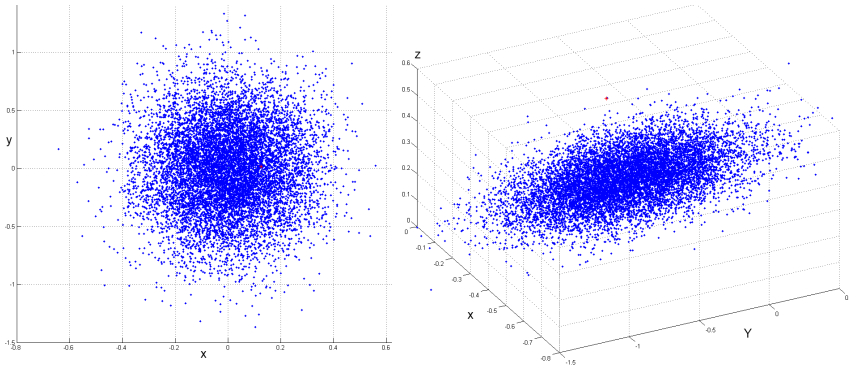
Figure 6

(a) The POI's position transformed to the coordinate space along axis *z*. (b) The distribution of the POI shows highly anisotropic distribution along axis *x*.

motion of the tool during the surgery is towards the directions with lower error distribution, the robot can speed up due to the lower error. Consequently, the optimal arrangement of the camera system can be given for each procedure, based on a pre-operative simulation and analysis.

5   Application to a Physical System

5.1   The JHU Image-Guided Neurosurgical System

A key aspect of these new techniques is to be applicable to existing systems, already deployed in ORs, or research laboratories. This require delicate proto-typing procedure and thorough testing on setups that well mimic the intended use.

We have developed the integrated surgical robotic system at the Johns Hopkins University (JHU, Baltimore, MD) to support skull base drilling. The system consists of a modified *NeuroMate* robot, a *StealthStation* (SS) surgical navigation device from Medtronic Navigation Inc. (Louisville, CO) and adequate network and control equipment (Fig. 7). The goal was to improve the safety and quality of neurosurgery while reducing the operating time. The robotized solution is only used for the removal of the bone tissue, to gain access to the anatomical region affected by a tumor or other lesions. Our technical approach was to use pre-operative imaging to identify the region of the skull base that could be safely drilled. We chose a cooperative control implementation (also called shared or compliant control), in which the surgeon applies forces to move the robot and the robot enforces the safety boundaries.

The JHU system has three major advantages. First, it offers advanced visual-ization features typical used in stereotactic surgery; the tool's position can be
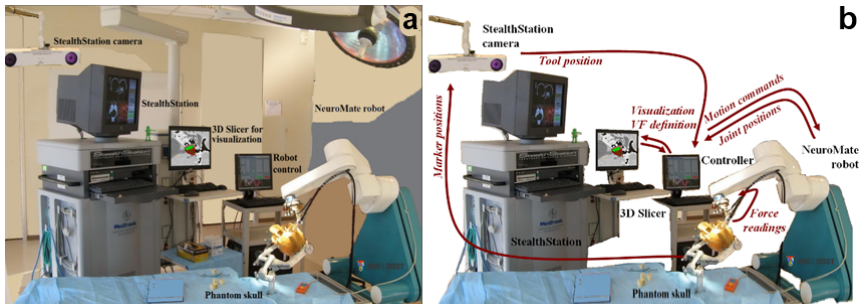
Figure 7
Hardware and software elements of the integrated neurosurgical system. (a) Physical arrangement of
the devices.
(b) Major flow of information between the system components.

followed on the 3D model of the patient, acquired from pre-operative CT scans.
Second, the surgical tool is mounted on the rigid robot, thereby improving its sta-
bility. The surgeons still hold the classic drill tool and directs its movement, but
they can release the tool any time. Finally, the most important advantage—and
the novelty of the application—is that the physician can define virtual boundaries
on the CT scan prior to the operation. This is called *Virtual Fixture*, and once reg-
istered to the robot, it is strictly enforced, thus preventing the tip of the tool from
going beyond the defined safe area.

5.2   JHU System Components

The system uses an FDA-approved *Medtronic StealthStation* for navigation. The
SS is only capable of tracking two rigid bodies at a time (one reference frame—
DRB and one tool—TRB), and there is an option to manually switch between
different reference frames and tools.

We use three different rigid bodies in our setup (two at a time):

- a *Tool Rigid Body* is fixed on the robot's end-effector (therefore specifically
  we may call it *Robot Rigid Body*),

- one is connected to the patient (e.g., at a *Mayfield head clamp*).

These two rigid bodies allow us to determine the robot's position with respect
to the skull. A third tool, a hand-held pointing probe is used to register the CT
image coordinates (the patient anatomy) to the Patient Image.

The tool serving as the end-effector is an *Anspach eMax 2* high-speed instrument
(The Anspach Effort Inc., Palm Beach Gardens, FL). The tool-holder (with rein-
forced bracket) is attached to the end of the NeuroMate through a force sensor,
a 6 DOF sensor (JR3 Inc., Woodland, CA). The system further integrates the
3D Slicer (*www.slicer.org*) software [39] for pre-operative planning and intra-
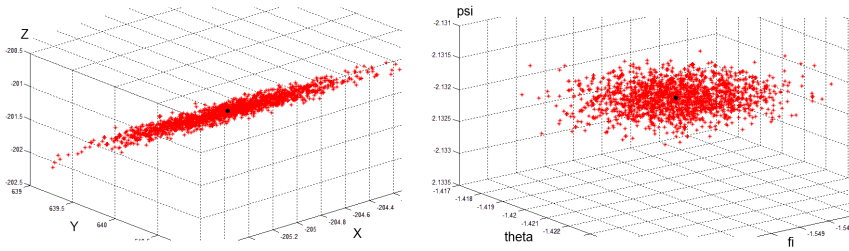operative visualization.

Figure 8

(a) The POI (tooltip) position transformed to the coordinate space of the patient on the real JHU setup. (b) The distribution of the rotation.

In the next step, I verified the concept on a real IG setup. The ongoing neurosurgical setup at JHU is a valid platform, complying with the standard description. While the previously presented error propagation approaches result in a moderately distorted POI distribution for a similar setup, in reality, measurements showed significant distortion of the error parameters for the actual robot tool. Fig. 8a shows the translational distribution, while Fig. 8b displays the angular distribution of the JHU system's drill. Principal component analysis showed that two components account for 99,7% of the variance in x, y, z directions and 98.6% of the rotations along x, y, z axes.

Conclusion

Effective mapping of spatial error based on a priori information is necessary to support the operation of computer-integrated medical devices. This is also in line with the most recent patient safety requirements and surgical robot standards. Generalized error values and the experience of the medical staff determines the use of a system under different conditions. The major focus of this research was to improve the theoretical tools and practical means available for accuracy assessment of interventional image-guided systems. The classical approach to simple 3D error theory is not sophisticated enough to ensure the highest level of safety for many advanced surgical robotic systems. A new concept was proposed— stochastic approach to determine the 6 DOF error distribution of a generic surgical robotic system. The method is based on the direct handling of the error distribution function and forbidden regions defined as a Virtual Fixture, and can provide the actual distribution of errors at the tool right before the intervention begins. This allows for the optimal placement of the devices in order to reduce the overall effect of navigation and registration errors. Simulation results showed the applicability of the theory, and computations have also been performed for the JHU robot system, where the inhomogeneity of the distribution along different axes was shown to be over a hundred fold, therefore seriously limiting the performance of the system. The error propagation simulation can provide im-

portant data on the accuracy of any surgical setup that may help manufacturers giving recommendations for improved operating room setups.

Acknowledgment

References

[1] A. Takács, D. Á. Nagy, I. Rudas, and T. Haidegger. Origins of surgical robotics: From space to the operating room. *Acta Polytechnica Hungarica*, 13(1):13–30, 2016.

[2] K. H. Wong. Imaging Modalities. In *Lecture Notes in Computer Science (LNCS), Proc. of the 1st Intl. Conf. on Information Processing in Computer-Assisted Interventions (IPCAI)*, pages 241–273, Geneva, 2010.

[3] J. Maintz and M. Viergever. A survey of medical image registration. *Medical Image Analysis*, 2(1):1–37, 1998.

[4] Y. Chen, I. Godage, H. Su, A. Song, and H. Yu. Stereotactic systems for mri-guided neurosurgeries: A state-of-the-art review. *Annals of biomedical engineering*, pages 1–19, 2018.

[5] C. Urban, P. Galambos, G. Györök, and T. Haidegger. Simulated medical ultrasound trainers a review of solutions and applications. *Acta Polytechnica Hungarica*, 15(7):111–133, 2018.

[6] M. Hoeckelmann, I. J. Rudas, P. Fiorini, F. Kirchner, and T. Haidegger. Current capabilities and development potential in surgical robotics. *Intl. J. of Advanced Robotic Systems*, 12(5):61, 2015.

[7] T. Haidegger. Autonomy for surgical robots: Concepts and paradigms. *IEEE Trans. on Medical Robotics and Bionics*, 1(2):65–76, 2019.

[8] P. Grunert, K. Darabi, J. Espinosa, and R. Filippi. Computer-aided navigation in neurosurgery. *Neurosurgical Review*, 26(2):73–99, 2003.

[9] P. Markelj, D. Tomaževič, B. Likar, and F. Pernuš. A review of 3d/2d registration methods for image-guided interventions. *Medical image analysis*, 16(3):642–661, 2012.

[10] A. I. Károly, R. Fullér, and P. Galambos. Unsupervised clustering for deep learning: A tutorial survey. *Acta Polytechnica Hungarica*, 15(8):29–53, 2018.

[11] D. Á. Nagy, I. J. Rudas, and T. Haidegger. Surgical data science, an emerging field of medicine. In *Neumann Colloquium (NC), 2017 IEEE 30th*, pages 000059–000064. IEEE, 2017.

[12] B. Gibaud, G. Forestier, C. Feldmann, G. Ferrigno, P. Gonçalves, T. Haidegger, C. Julliard, D. Katić, H. Kenngott, L. Maier-Hein, et al. Toward a standard ontology of surgical process models. *International journal of computer assisted radiology and surgery*, 13(9):1397–1408, 2018.

[13] T. Jacobs, J. Veneman, G. S. Virk, and T. Haidegger. The flourishing landscape of robot standardization [industrial activities]. *IEEE Robotics & Automation Magazine*, 25(1):8–15, 2018.

[14] T. Haidegger, S. Győri, B. Benyó, and Z. Benyó. Stochastic approach to error estimation for image-guided robotic systems. In *Engineering in Medicine and Biology Society (EMBC), 2010 Annual International Conference of the IEEE*, pages 984–987. IEEE, 2010.

[15] T. Haidegger, P. Kazanzides, B. Benyó, L. Kovács, and Z. Benyó. Surgical case identification for an image-guided interventional system. In *Proc. of the IEEE/RSJ Intl. Conf. on Intelligent Robots and Systems (IROS)*, Taipei, 2010.

[16] T. Haidegger, P. Kazanzides, I. Rudas, B. Benyó, and Z. Benyó. The importance of accuracy measurement standards for computer-integrated interventional systems. In *EURON GEM Sig Workshop on The Role of Experiments in Robotics Research at IEEE ICRA*, pages 1–6, 2010.

[17] D. Y. Hsu. *Spatial Error Analysis*. Wiley–IEEE, New York, NY, 1998.

[18] C. R. Maurer, J. M. Fitzpatrick, M. Y. Wang, R. L. Galloway, R. J. Maciunas, and G. S. Allen. Registration of head volume images using implantable fiducial markers. *IEEE Trans. on Medical Imaging*, 16(4):447–462, 1997.

[19] J. M. Fitzpatrick, J. B. West, and C. R. Maurer. Predicting Error in Rigid-Body Point-Based Registration. *IEEE Trans. on Medical Imaging*, 17(5):694–702, 1998.

[20] J. M. Fitzpatrick. Fiducial registration error and target registration error are uncorrelated. In *Proc. of SPIE Medical Imaging*, volume 7261, pages 1–12, Orlando, FL, 2009.

[21] A. Danilchenko and J. M. Fitzpatrick. General approach to error prediction in point registration. In *Proc. of SPIE Medical Imaging*, volume 7625–0F, pages 1–14, San Diego, CA, 2010.

[22] T. Haidegger. *Theory and method to enhance computer-integrated surgical systems*. PhD thesis, in electrical engineering, 2011.

[23] T. Haidegger, P. Kazanzides, I. Rudas, B. Benyó, and Z. Benyó. The Importance of Accuracy Measurement Standards for Computer-Integrated Interventional Systems. In *Proc. of the EURON GEM Sig Workshop on The Role of Experiments in Robotics Research at IEEE ICRA*, pages 19–24, Anchorage, AK, 2010.

[24] G. Widmann, R. Stoffner, M. Sieb, and R. Bale. Target registration and target positioning errors in computer-assisted neurosurgery. *Intl. J. of Medical Robotics and Computer Assisted Surgery*, 5(4):355–365, 2009.

[25] J. M. Fitzpatrick. The role of registration in accurate surgical guidance. *Proc. of the Institution of Mechanical Engineers, Part H: J. of Engineering in Medicine*, 224(5):607–622, 2010.

[26] D. M. Kwartowitz, S. D. Herrell, and R. L. Galloway. Toward image-guided robotic surgery: determining intrinsic accuracy of the da Vinci robot. *Intl. J. of Computer Assisted Radiology and Surgery*, 1(3):157–165, 2006.

[27] M. Kuhn, M. Jablonowski, P. Gieles, M. Fuchs, and H.-A. Wischmann. A Unifying Framework for Accuracy Analysis in Image-Guided Surgery. In *Proc. of the Annual Intl. Conf. of the IEEE Engineering in Medicine and Biology Society (EMBC)*, pages 238–240, Amsterdam, 1996.

[28] R. H. Taylor and P. Kazanzides. Medical Robotics and Computer-Integrated Interventional Medicine. *Advances in Computers: Emerging Technologies*, 73:219–258, 2008.

[29] M. H. Moghari, B. Ma, and P. Abolmaesumi. A theoretical comparison of different target registration error estimators. In *Lecture Notes in Computer Science (LNCS), Proc. of the Annual Conf. of the Medical Image Computing and Computer Assisted Intervention Society (MICCAI)*, volume 5424, pages 1032–1040, New York, NY, 2008.

[30] M. H. Moghari and P. Abolmaesumi. A high-order solution for the distribution of target registration error in rigid-body point-based registration. In *Lecture Notes in Computer Science (LNCS), Proc. of the Annual Conf. of the Medical Image Computing and Computer Assisted Intervention Society (MICCAI)*, volume 9, pages 603–611, Kobenhavn, 2006.

[31] W. Zylka, J. Sabczynski, and G. Schmitz. A Gaussian approach for the calculation of the accuracy of stereotactic frame systems. *J. Medical Physics*, 26(3):381–392, 1999.

[32] A. D. Wiles, D. G. Thompsona, and D. D. Frantz. Accuracy assessment and interpretation for optical tracking systems. In *Proc. of SPIE Medical Imaging*, volume 5367, pages 421–432, San Diego, CA, 2004.

[33] R. Khadem, C. C. Yeh, M. Sadeghi-tehrani, M. R. Bax, J. A. Johnson, J. N. Welch, E. P. Wilkinson, and R. Shahidi. Comparative tracking error analysis of five different optical tracking systems. *Computer Aided Surgery*, 5(2):98–107, 2000.

[34] B. Allen and G. Welch. A general method for comparing the expected performance of tracking and motion capture systems. In *Proc. of the ACM Symp. on VR Software and Technology*, pages 210–220, Monterey, CA, 2005.

[35] W. Hoff and T. Vincent. Analysis of Head Pose Accuracy in Augmented Reality. *IEEE Trans. on Visualization and Computer Graphics*, 6(4):319–334, 2000.

[36] T. Sielhorst, M. Bauer, O. Wenisch, G. Klinker, and N. Navab. Online Estimation of the Target Registration Error for n-Ocular Optical Tracking Systems. In *Lecture Notes in Computer Science (LNCS), Proc. of the Annual*

Conf. of the Medical Image Computing and Computer Assisted Intervention Society (MICCAI), volume 4792, pages 652–659, Brisbane, 2007.

[37] M. Bauer, M. Schlegel, D. Pustka, N. Navab, and G. Klinker. Predicting and estimating the accuracy of n-occular optical tracking systems. In *Proc. of the 5th IEEE/ACM Intl. Symp. on Mixed and Augmented Reality (ISMAR)*, pages 43–51, Santa Barbara, 2006.

[38] T. Xia, C. Baird, G. Jallo, K. Hayes, N. Nakajima, N. Hata, and P. Kazanzides. An integrated system for planning, navigation and robotic assistance for skull base surgery. *Intl. J. of Medical Robotics and Computer Assisted Surgery*, 4(4):321–330, 2008.

[39] S. Pieper, M. Halle, and R. Kikinis. 3D Slicer. In *IEEE Intl. Symp. on Biomedical Imaging*, pages 632–635, Arlington, VA, 2004.